PHOTONICS Research

Active stabilization of terahertz waveforms radiated from a two-color air plasma

Yonghao Mi,[1,3] Kyle Johnston,[1] Valentina Shumakova,[1] Søren H. Møller,[1] Kamalesh Jana,[1] Chunmei Zhang,[1] André Staudte,[1] Shawn Sederberg,[1,2,*] and Paul B. Corkum[1]

[1]Joint Attosecond Science Laboratory, University of Ottawa and National Research Council Canada, Ottawa, Ontario K1N 6X1, Canada
[2]Present address: School of Engineering Science, Simon Fraser University, Burnaby, British Columbia V5A 1S6, Canada
[3]e-mail: ymi@uottawa.ca
*Corresponding author: shawn_sederberg@sfu.ca

Received 16 June 2021; revised 28 October 2021; accepted 31 October 2021; posted 2 November 2021 (Doc. ID 434325); published 13 December 2021

Intense laser fields focused into ambient air can be used to generate high-bandwidth current densities in the form of plasma channels and filaments. Excitation with bichromatic fields enables us to adjust the amplitude and sign of these currents using the relative phase between the two light pulses. Two-color filamentation in gas targets provides a route to scaling the energy of terahertz pulses to microjoule levels by driving the plasma channel with a high-energy laser source. However, the structure of plasma channels is highly susceptible to drifts in both the relative phase and other laser parameters, making control over the waveform of the radiated terahertz fields delicate. We establish a clear link between the phase dependence of plasma currents and terahertz radiation by comparing *in situ* detection of current densities and far-field detection of terahertz electric fields. We show that the current measurement can be used as a feedback parameter for stabilizing the terahertz waveform. This approach provides a route to energetic terahertz pulses with exceptional waveform stability.

https://doi.org/10.1364/PRJ.434325

1. INTRODUCTION

Fine control of time-varying currents enables precise sculpting of electromagnetic radiation. However, technical challenges in scaling conventional electronic oscillators to terahertz (THz) frequencies call for alternative approaches to generate THz radiation. When femtosecond laser pulses are applied to optoelectronic processes, currents can be modulated on femtosecond time scales. Transient currents can be optically excited using photoconductive switches [1–4], quantum interference current injection in semiconductors [5–8], strong-field current injection in dielectrics and monolayers [9–11], or in a laser-ignited plasma channel or filament [12–18]. Depending on the configuration, the spectral content of the resulting THz radiation can extend from approximately 0.1 THz up to the inverse of the laser pulse duration, $1/\tau_p$.

Over the last two decades, several solid-state platforms for generating intense THz pulses have emerged, including tilted-pulse-front excitation of $LiNbO_3$ crystals [19–21], optical rectification in large-aperture ZnTe or organic crystals [22,23], and large-aperture photoconductive switches [24]. Scaling the energy of THz currents and radiation using solid-state platforms is ultimately restricted by electrical or optical breakdown, leading to permanent damage, and by the availability of crystals with ever-larger apertures. In contrast, plasma channels and filaments excited in gases or liquids rely on optical breakdown and are continuously replenished, providing a highly scalable platform for THz generation [25,26]. Although THz radiation can be observed when a plasma channel is driven by a single femtosecond laser pulse, stronger electric-field asymmetry is possible using a bichromatic or few-cycle pulse excitation, leading to higher peak currents and stronger THz radiation.

In two-color plasma formation, a fundamental laser pulse [ω, typically carried at a wavelength lying within the near- or mid-infrared (mid-IR) spectral region] and its second harmonic (2ω) are focused collinearly into a medium. The bichromatic field is intense enough to ionize the medium and to impart the resulting electron wave packets with significant momentum. Both the time-dependent ionization rate and the subsequent electron wave packet dynamics can be controlled by adjusting the relative phase between the two pulses, $\Delta\varphi_{\omega,2\omega} = 2\varphi_\omega - \varphi_{2\omega}$. Coherent control on a microscopic scale leads to macroscopic dynamic currents, which radiate a THz pulse.

Through a quantum mechanical treatment and complementary experiments, Karpowicz and Zhang have demonstrated two linked processes that contribute to the radiated THz

fields [27]. The first arises from the initial acceleration of the electron wave packets by the optical fields. Subsequent to acceleration, each electron wave packet propagates freely until it undergoes a collision with a neighboring atom or molecule, giving rise to bremsstrahlung, the second contribution to the radiated THz fields. Using $\Delta\varphi_{\omega,2\omega}$ to precisely manipulate the electron wave packet dynamics provides complementary control over the amplitude and polarity of the THz radiation. Applying two-color mid-IR fields to plasma formation in ambient air has enabled the generation of broadband THz fields with amplitudes above 100 MV $\cdot$ cm^{-1} [25].

Freedom to optimize the focusing geometry, energy, polarization, duration, and spatial structure of each of the two pulses is gained when they are diverted into separate arms of an interferometer [16,28,29]. Independent control over the pulse properties of ω and 2ω in the interferometer is necessary to generate, for example, THz fields with a circular or more complex polarization state, or by mid-IR driver pulses, where zeroth-order half- and quarter- wave plates are not readily available. This provides additional opportunities for improving THz conversion efficiencies, as demonstrated with circularly polarized ω and 2ω laser pulses in Ref. [29]. At the same time, a two-color interferometer introduces the need for extreme mechanical stability. Critically, any interferometric drift will change $\Delta\varphi_{\omega,2\omega}$, which will influence the plasma currents and the radiated THz waveform.

Due to the reliance of laser-excited plasma channels and filaments on strong-field ionization, the peak plasma density and length of the channel can be sensitive to instabilities in the driving light or the surrounding environment. Notably, a plasma channel constitutes a highly dispersive medium, leading to a phase slip in $\Delta\varphi_{\omega,2\omega}$ as the bichromatic fields propagate through it. The total change in $\Delta\varphi_{\omega,2\omega}$ that accumulates in the plasma channel will be sensitive to instabilities in the laser source (i.e., the ω and 2ω fields themselves) or surrounding environment.

Recently, laser-excited currents measured in ambient air have been used to characterize the carrier-envelope phase of laser pulses [30] and to sample the vector potential of visible-to-mid-IR laser fields [31,32]. Direct optoelectronic detection of currents excited in a plasma channel also provides an *in situ* probe of the plasma currents that ultimately radiate a THz impulse, and it can be expected that plasma currents and THz radiation share a mutual dependency on $\Delta\varphi_{\omega,2\omega}$ and its fluctuations. *In situ* current detection would also provide a means to probe the coherent evolution of the bichromatic fields within the plasma channel and could potentially provide insight into decoherence mechanisms in laser-excited plasmas.

In this work, we simultaneously measure the phase dependency of optically excited currents in a plasma channel and the peak electric field of the emitted THz waveform. We demonstrate that under certain conditions, both signals are strongly correlated and are influenced similarly by instabilities in $\Delta\varphi_{\omega,2\omega}$. Using the measured current signal as a two-color phase detector, we correct for instabilities in the THz waveform arising from both the two-color interferometer and the plasma environment in real time. This approach demonstrates a potential scheme for generating energetic THz pulses derived from plasma channels with extreme waveform stability.

2. EXPERIMENTAL SETUP

The experimental configuration is shown in Fig. 1(a). One output beam from a Legend Elite Duo amplifier (wavelength, $\lambda = 800$ nm, pulse energy, $E_p = 4.5$ mJ, pulse duration, $\tau_p = 30$ fs, repetition rate, $f_{\text{rep}} = 1$ kHz) is first split into a strong (95%) pulse for THz generation and a weak (5%) probe pulse for electro-optic sampling (EOS). The strong pulse (ω) is transmitted through a β-barium-borate (BBO) crystal for generating the second-harmonic beam (2ω), and the two colors are split into separate optical paths using a dichroic mirror (DM). The ω and 2ω pulses each pass through a half-wave plate (HWP) and a wire-grid polarizer (WGP) to enable independent optimization of the pulse energy and polarization of each beam. In addition, the ω beam is reflected from two mirrors mounted to a delay stage with a piezoelectric actuator, enabling precise control over $\Delta\varphi_{\omega,2\omega}$.

The two pulses are then recombined collinearly using a DM and focused into ambient air with an $f = 250$ mm spherical mirror. A 150-μm-thick glass coverslip is introduced into the optical path approximately halfway between the focusing mirror and the focal plane. The pulses transmitted through the glass coverslip excite a plasma channel in ambient air. Typical pulse energies used to generate the plasma channel are $E_{p,\omega} = 0.44$ mJ for the ω beam and $E_{p,2\omega} = 0.28$ mJ for the 2ω beam. Notably, the corresponding peak powers ($P_{p,\omega} \sim 13$ GW for ω and $P_{p,2\omega} \sim 4.9$ GW for 2ω) exceed the critical power for self-focusing in ambient air, and the plasma formation is in the filamentation regime. Although we have not side-imaged visible light emission from the plasma channel, we estimate the length of the plasma channel to be approximately 6.5 ± 0.5 mm. Femtosecond laser pulses with similar peak power and focusing geometry undergoing filamentation typically produce plasma columns with ~100 μm diameters [33]. THz emission arising from the plasma currents is collected and collimated using an off-axis parabolic mirror (effective focal length, 150 mm). The THz pulse energy is measured to be approximately $E_{\text{THz}} = 25$ nJ using a pyroelectric detector (Gentec-EO, THZ9B-BL-DZ-DO), with a corresponding conversion efficiency, $\eta = 3.5 \times 10^{-5}$.

The energy of the probe beam is adjusted using a neutral density filter wheel (ND), and its polarization is corrected with a WGP. Its arrival time relative to the THz pulse is controlled using a motorized delay stage. The THz pulse and the probe pulse are combined collinearly with a bare silicon wafer (Si), which simultaneously absorbs the ω and 2ω beams, and are subsequently focused through a 1-mm-thick ZnTe crystal for EOS. A standard balanced photodetection setup consisting of a quarter-wave plate (QWP), Wollaston prism (WP), and a pair of photodiodes connected to a lock-in amplifier (Stanford Research Systems, SR830) is used to read out the polarization rotation of the probe in response to the THz electric fields. The measurements presented in this work are acquired using a lock-in time constant of $\tau = 100$ ms. The THz waveform that is measured can be viewed as a probe for $\Delta\varphi_{\omega,2\omega}$ after it has been influenced by all sources of instability in the optical paths.

The weak reflections of the two beams from the glass CS are transmitted through a second BBO crystal, which frequency-doubles the ω light. Interference fringes between

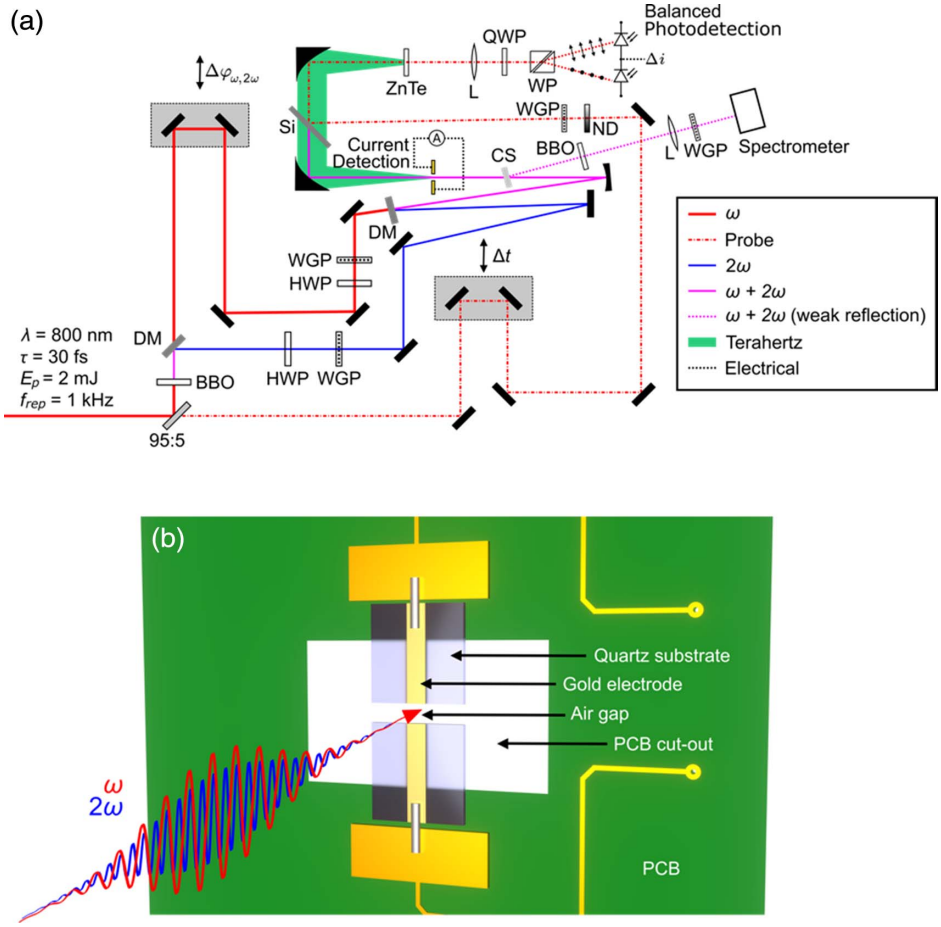

Fig. 1. (a) Schematic of the experimental setup. An $\omega - 2\omega$ pulse pair is focused into ambient air and a plasma channel is formed. The radiated THz waveform is collected and sampled via EOS. Two diagnostic tools enable insight into the origin of interferometric drifts between the ω and 2ω pulses: spectral interference and *in situ* detection of current densities generated in the plasma channel. (b) Rendering of the detector used to sample currents within the plasma channel; the detector is placed near the focal plane of the bichromatic pulses. The separation between the electrodes is approximately 1 mm and is sufficiently large that neither the optical beams nor the THz pulses are impeded by the electrodes. PCB, printed circuit board; L, focusing lens.

the two sources of 2ω light, originating from the two arms of the interferometer, are then observed using a spectrometer. In this arrangement, shifts in the position of the interference maxima and minima over time relate directly to phase instabilities in the two-color interferometer. This detection scheme serves as a probe for coherence in the bichromatic fields that is established in the two-color interferometer.

In addition, a pair of gold electrodes deposited onto separate quartz substrates is mounted to a printed circuit board, such that they are separated by an air gap approximately 1-mm wide, shown schematically in Fig. 1(b). When this detector is positioned near the focal plane of the optical beams, neither the plasma generation nor the measured THz radiation is altered in any way. Currents excited in the plasma channel can easily be measured with this detector using a second lock-in amplifier. *In situ* detection of phase-dependent currents provides a means to relate the THz waveform emitted from the plasma channel to coherence in the bichromatic fields emerging from the two-color interferometer.

3. RESULTS AND DISCUSSION

A. Free-Running THz Waveform Measurements

To investigate the feasibility of generating stable THz waveforms using this configuration, we record 20 sequential EOS scans, a measurement that lasts a total of approximately 45 min. The waveforms obtained in scans 1, 10, and 20 are shown in Figs. 2(a)–2(c), respectively. To quantify drifts in the waveform over time, we calculate the normalized root mean square error (RMSE) between the initial waveform and each subsequent scan,

$$\mathrm{RMSE}_i = \frac{1}{E_{1,\max}} \sqrt{\frac{\sum_{n=1}^{N} (E_{i,n} - E_{1,n})^2}{N}}. \tag{1}$$

In this expression, N is the number of data points that make up each EOS scan, i is the scan number, n is the data point number within a scan, E_1 is the initial waveform that was measured, E_i is the ith waveform that was recorded, and $E_{1,\max}$ is

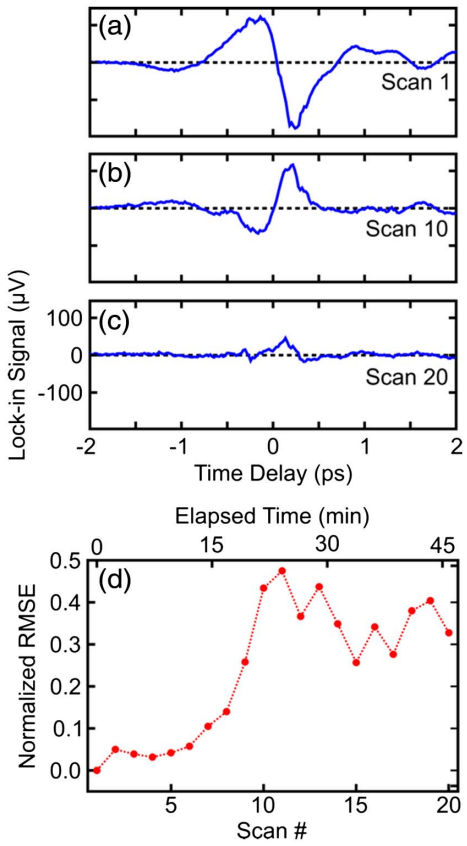

Fig. 2. Collection of THz pulses measured under ambient lab conditions, demonstrating the extreme sensitivity of the THz waveform to interferometric, laser, and environmental instabilities. The scan is repeated 20 times and the first, tenth, and twentieth waveforms are shown in (a)–(c), respectively. The normalized root mean square error between the first scan and each subsequent scan is shown in (d).

the normalization constant, which we take to be the peak amplitude of the initial THz waveform.

Figure 2(d) shows the calculated RMSE for each of the 20 scans. In this data set, the waveform is relatively stable for the first six scans, but experiences considerable drifts thereafter. From these measurements, it is clear that using this configuration makes long-term THz waveform stability a challenge.

B. Investigating the Origins of THz Waveform Instabilities

Next, we control the relative-phase-dependent THz waveform using the piezoelectric actuator and record its peak electric-field amplitude at a fixed probe delay. We limit the extent to which the plasma environment influences the current measurement by positioning the current detector near the beginning of the plasma channel. Then we simultaneously record the 2ω interference spectrum, current, and the EOS signal as $\Delta\varphi_{\omega,2\omega}$ is adjusted over a range of approximately 375 rad. Here, we define $\Delta\varphi_{\omega,2\omega}$ as the relative phase introduced to the two-color interferometer by the piezo-actuated delay stage; it does not account for any drifts in the interferometer. Therefore, analyzing changes in the scans over time provides insight into interferometric instabilities. An exemplary scan is plotted in Fig. 3(a) and, as expected, each parameter undergoes periodic oscillations at the 2ω frequency as $\Delta\varphi_{\omega,2\omega}$ is increased. Figure 3(b) displays the envelopes extracted from the current and THz measurements, and it is determined that the center of mass of the THz envelope is advanced by 25.7 rad with respect to that of the current envelope.

Due to plasma dispersion, $\Delta\varphi_{\omega,2\omega}$ evolves along the length of the plasma channel. Positioning the current detector at a certain plane, $z = z_0$, within the plasma channel enables the local $\Delta\varphi_{\omega,2\omega}$ to be sampled. Conversely, the collection parabolic mirror collimates the THz waveform emitted from the region of the plasma channel near its focal plane. In general, what is detected is a weighted average of the waveforms emitted from each element along the plasma channel, where strong electric fields radiated from a position close to the focal plane of the parabolic mirror contribute substantially to the measured THz waveform. The envelope offset shown in Fig. 3(b) arises from plasma dispersion that accumulates between z_0 and the region from which the strongest THz emission is collected. We take the envelope offset to be a measure of the position of the current detector within the plasma channel.

After repeating the scan 15 times, we examine the relative phase between the oscillations comprising each measurement and calculate their correlation over subsequent scans. The evolution of the phase-dependent EOS, current, and 2ω spectral interference measurements over the duration of the 15 scans is shown in Figs. 3(c)–3(e), respectively. Figure 3(f) displays the phase of each measurement for a fixed position of the piezoelectric actuator, corresponding to $\Delta\varphi_{\omega,2\omega} = -13.9$ rad. This value was chosen because it is close to the maximum of the EOS envelope shown in Fig. 3(b) and, therefore, provides THz pulses with the highest signal-to-noise ratio (SNR). For clarity, we have added a constant offset to each data set in order to make its average value zero. Each of the three measurements displays a trend with qualitative similarities. However, numerical analysis of the data reveals that the strongest correlation among any of the three measurements lies between the current and the 2ω spectral interference. The differences between the current and 2ω spectral interference phases, and between the current and THz phases, are calculated and plotted on the right-hand axis of Fig. 3(f). The RMSE between the current and 2ω spectral interference phases is calculated to be 139 mrad. Similarly, the RMSE between the current and THz phases is found to be 400 mrad.

The close correlation between the current signal and the 2ω spectral interference signal near the beginning of the plasma channel signifies that, in this detection plane, drifts in the phase-dependent plasma currents are primarily linked to interferometric instabilities. Here, the bichromatic fields have only interacted with a small fraction of the plasma channel, and $\Delta\varphi_{\omega,2\omega}$ has not yet been significantly influenced by instabilities in the plasma. The weaker link between the current measurement and the THz signal demonstrates that significant instability to $\Delta\varphi_{\omega,2\omega}$ accumulates as the bichromatic fields experience the plasma situated between the current detection plane and the plane from which the strongest THz emission is collected. Therefore, it is advantageous to probe currents generated in the middle or latter half of the plasma channel, where

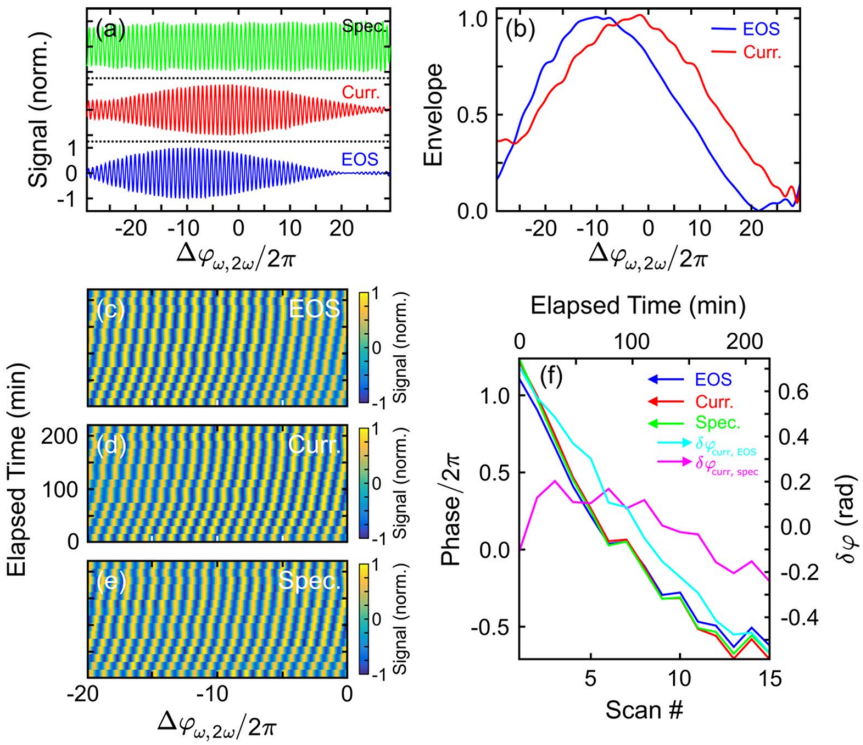

Fig. 3. Phase-sensitivity correlations between the THz waveform and currents measured slightly before the center of the plasma channel. (a) Simultaneous measurements of the peak of the THz waveform (blue), the current (red), and the 2ω spectral interference signal as $\Delta\varphi_{\omega,2\omega}$ is adjusted. (b) The envelope functions corresponding to the THz waveform (blue) and current (red) measurement presented in (a), extracted via Hilbert transformation. The scan shown in (a) is repeated 15 times, and the data obtained from EOS, the current detector, and 2ω spectral interference are shown in (c), (d), and (e), respectively. (f) Summary of the phase correlation between the THz emission (blue), currents (red), and the spectral interference signal (green); the error between the phases of the current and the THz signal, $\delta\varphi_{\mathrm{curr,EOS}}$ (cyan), and the error between the phases of the current and spectral interference signals, $\delta\varphi_{\mathrm{curr,spec}}$ (magenta), are plotted using the axis on the right-hand side. The root mean square of $\delta\varphi_{\mathrm{curr,EOS}}$ is calculated to be 400 mrad, whereas the root mean square of $\delta\varphi_{\mathrm{curr,spec}}$ is found to be 139 mrad.

signatures of the plasma environment have been imprinted onto $\Delta\varphi_{\omega,2\omega}$.

C. Strengthening the Correlation between Currents and THz Radiation

Given that phase drifts arising from the plasma channel can be significant and these are not detected using the 2ω spectral interference signal, we now focus exclusively on using the current detector as an all-encompassing probe for instabilities in $\Delta\varphi_{\omega,2\omega}$. The current detector is shifted into the region of the plasma channel from which the strongest side-emitted visible light is observed, where the highest current densities exist. In a similar manner, we measure the currents excited in the plasma channel and the peak amplitude of the THz waveform as $\Delta\varphi_{\omega,2\omega}$ is adjusted. An exemplary scan showing the two measurements is plotted in Fig. 4(a). Figure 4(b) displays the envelope extracted from each measurement, and it is determined that the centers of mass of the two envelopes are now separated by only 13.4 rad.

This scan is repeated 20 times, lasting a total of approximately 130 min. By extracting the phase of each scan at a fixed $\Delta\varphi_{\omega,2\omega} = -12.8$ rad, we directly examine the correlation between drifts in the phase dependency of the two signals over the duration of the 20 scans. As before, this value of $\Delta\varphi_{\omega,2\omega}$ was chosen because it produces a THz pulse with near-optimal SNR. The phase drift of the two signals as well as their difference is shown in Fig. 4(c). The RMSE between the two phases is calculated to be 57.1 mrad. This seven-fold improvement in the RMSE between the phase sensitivity of the current and EOS measurements with respect to that measured in the previous section introduces the possibility of using one measurement as a detector for $\Delta\varphi_{\omega,2\omega}$ that can in turn be used to stabilize the other.

D. Stabilization of THz Waveforms

In the interest of generating THz fields with long-term waveform stability, we continuously sample the current, and use a software-based feedback loop to stabilize the current value by adjusting $\Delta\varphi_{\omega,2\omega}$ using the piezoelectric-actuated delay stage. The detection and feedback scheme is illustrated schematically in Fig. 5(a). Prior to engaging the feedback loop, the program conducts a scan of $\Delta\varphi_{\omega,2\omega}$ over approximately 4π rad in order to measure the maximum and minimum current amplitudes. Upon entering the feedback loop, it reads out the current once per second and compares it with the value measured in the initial position. If the error exceeds a certain threshold, it steps the piezoelectric actuator in the appropriate direction until the error value is reduced below the threshold. Due to the relatively

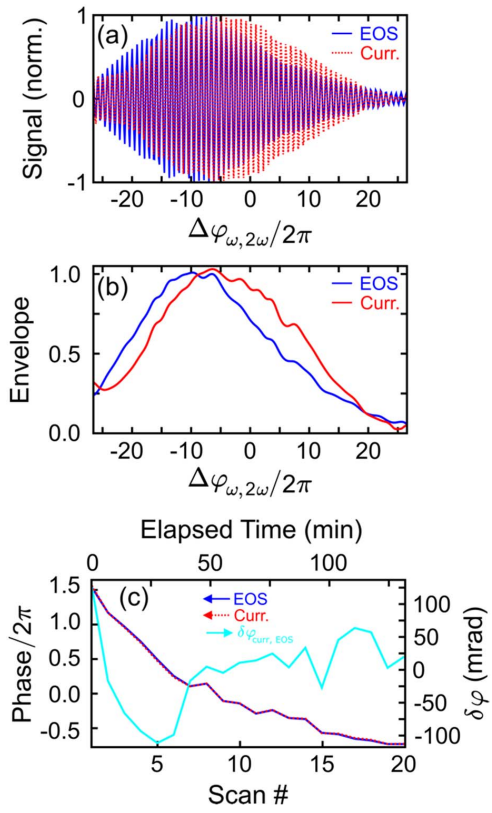

Fig. 4. Measurement of correlations in phase sensitivity of the THz waveform and currents performed at the position in the plasma channel from which the brightest side-emitted light is observed. (a) Dependency of the peak of the THz waveform (blue) and the current (red) on $\Delta\varphi_{\omega,2\omega}$, where sensitive control over the amplitude and sign of both parameters is demonstrated; (b) envelope functions of the measured data in (a), extracted via Hilbert transformation. Notably, the center of mass of the EOS envelope is advanced in phase by approximately 13.4 rad with respect to the center of mass of the current envelope. This shift is a direct consequence of plasma dispersion within the plasma channel. Only a portion of this plasma dispersion is experienced by the time pulses arriving at the current detector, whereas THz emission continues at subsequent positions along the plasma channel. (c) Summary of the phase correlation between currents and THz emission. The phase of the oscillating current (red) and THz emission (blue) is extracted from each scan for $\Delta\varphi_{\omega,2\omega} = -12.8$ rad, where a constant offset between the two parameters is removed. The error between these two parameters is shown by the green curve, which has a root mean square error of 57.1 mrad.

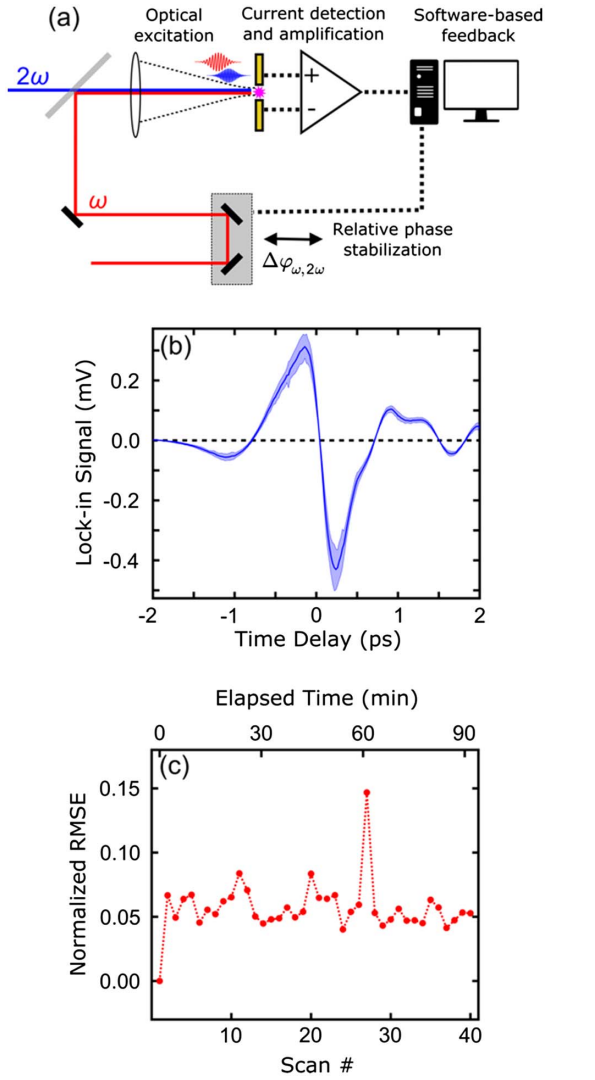

Fig. 5. THz waveform stabilization. (a) Schematic of the current detection and feedback scheme. The average of 40 scans of the stabilized THz waveform is shown by the solid line in (b), and the $1-\sigma$ standard deviation is depicted by the shaded regions. (c) The normalized root mean square error of each scan with respect to the first scan.

slow response time of this feedback loop, it is primarily effective at stabilizing slow drifts in the two-color interferometer or in the laser parameters. Corrections to impulsive instabilities, such as vibrational shocks introduced to the optical table, are slower, and these events can introduce significant distortions to the measured waveforms.

We perform 40 scans of the THz waveform, lasting a total of approximately 90 min, and plot the mean waveform together with error margins representing the $1-\sigma$ standard deviation of the measurements in Fig. 5(b). As before, we calculate the normalized RMSE between the first scan and each subsequent scan, which is shown in Fig. 5(c). With the exception of one waveform, the RMSE is maintained at approximately 0.05. Even when exposed to vibrational perturbations by the work of another researcher, the RMSE never exceeds 0.15.

Overall, the feedback scheme is successful in stabilizing the THz waveform over the duration of the scans, and it is expected that this could be extended to considerably longer time intervals. Here, we have focused on demonstrating the utility of this approach through optical measurements. We note that improving the feedback scheme using analog electronics and more advanced algorithms could lead to a significant reduction in the error margins and an improved response to impulsive instabilities.

4. CONCLUSION AND OUTLOOK

We have presented a straightforward and robust technique for monitoring fluctuations in $\Delta\varphi_{\omega,2\omega}$ when bichromatic laser

fields are applied to the formation of plasma channels in air and THz generation. Since contributions to the observed waveform instabilities arise from both the two-color interferometer and the plasma channel, it is anticipated that this scheme will be useful for both "in-line" and interferometric approaches to generating THz radiation from plasma channels. A direct outcome of this stabilization scheme will be energetic THz pulses with highly stable waveforms. Using shorter ω and 2ω pulses will enable generation and sampling of broadband light spanning the entire infrared spectral region, expanding the scope of applications of the radiated electromagnetic waves [34,35].

A robust scheme enabling independent manipulation of the ω and 2ω beams opens up the possibility to spatially structure each color and to drive laser-ignited plasmas using structured light pulses. The ability to do so would enable ambient air to be used as a platform for three-dimensional active metaoptical current structures. Controlling intricate current arrangements contained in the plasma channel would facilitate vectorization, spatial structuring, beam steering, and phase front control of the resulting THz radiation without requiring sophisticated nanostructures, in a manner that is similar to what has recently been demonstrated using two-color-injected semiconductor currents [36–38]. Implementing a two-color scheme using ultraviolet light could provide a route to current control on 100-nm scales.

Spatial structuring of THz fields could also be exploited to launch exotic electromagnetic pulses, such as a "flying torus" [39]. Furthermore, the direct link between currents and magnetic fields would enable intricate control of magnetic fields within the plasma channel and of the radiated THz pulses. While magnetic fields on the order of 100 T have been observed in dense plasmas excited by relativistic laser pulses, these fields have conventionally been challenging to access and use [40,41]. Applying intense structured light beams to similar experiments could enable current densities in the form of ring currents to be driven, providing spatial separation between the currents and magnetic fields. These magnetic fields could potentially be used to guide relativistic electron beams.

Conventionally, information about plasma channels and filaments can only be extracted using external measurements. This *in situ* current detection scheme provides direct access to currents within plasma channels and filaments. We anticipate that this approach could be used to spatially map current densities within filaments in order to provide fundamental insight into the processes that govern their formation. Finally, for sufficiently long or dense plasma channels, the detection of currents along the length of the plasma channel would enable direct visualization of the buildup of decoherence along its length. Measuring the conditions under which decoherence accumulates rapidly would provide an understanding of the ultimate limits of coherent control as applied to filamentation.

Funding. Canada Research Chairs; Natural Sciences and Engineering Research Council of Canada; Army Research Office (W911NF-19-1-0211); Defense Advanced Research Projects Agency (D18AC00011); Deutsche Forschungsgemeinschaft (MI 2434/1-1).

Acknowledgment. The authors are grateful for stimulating discussions with Aleksey Korobenko, Mathew Britton, Shima Gholam-Mirzaei, Mojtaba Taheri, Andrei Naumov, David Villeneuve, Saroj Tripathi, Wei Cui, and Jean-Michel Ménard. Y. M. acknowledges support from the Deutsche Forschungsgemeinschaft (German Research Foundation).

Disclosures. The authors declare no conflicts of interest.

Data Availability. Data underlying the results presented in this paper may be obtained from the authors upon reasonable request.

REFERENCES

1. G. Mourou, V. V. Stancampiano, A. Antonetti, and A. Orszag, "Picosecond microwave pulses generated with a picosecond laser-driven semiconductor switch," Appl. Phys. Lett. **39**, 295–296 (1981).
2. D. H. Auston and P. R. Smith, "Generation and detection of millimeter waves by picosecond photoconductivity," Appl. Phys. Lett. **43**, 631–633 (1983).
3. D. H. Auston, K. P. Cheung, and P. R. Smith, "Picosecond photoconducting Hertzian dipoles," Appl. Phys. Lett. **45**, 284–286 (1984).
4. P. R. Smith, D. H. Auston, and M. C. Nuss, "Subpicosecond photoconducting dipole antennas," IEEE J. Quantum Electron. **24**, 255–260 (1988).
5. E. Dupont, P. B. Corkum, H. C. Liu, M. Buchanan, and Z. R. Wasiliewski, "Phase-controlled currents in semiconductors," Phys. Rev. Lett. **74**, 3596–3599 (1995).
6. R. Atanasov, A. Haché, J. L. P. Hughes, H. M. van Driel, and J. E. Sipe, "Coherent control of photocurrent generation in bulk semiconductors," Phys. Rev. Lett. **76**, 1703–1706 (1996).
7. A. Haché, Y. Kostoulas, R. Atanasov, J. L. P. Hughes, J. E. Sipe, and H. M. van Driel, "Observation of coherently controlled photocurrent in unbiased, bulk GaAs," Phys. Rev. Lett. **78**, 306–309 (1997).
8. A. Haché, J. E. Sipe, and H. M. van Driel, "Quantum interference control of electrical currents in GaAs," IEEE J. Quantum Electron. **34**, 1144–1154 (1998).
9. A. Schiffrin, T. Paasch-Colberg, N. Karpowicz, V. Apalkov, D. Gerster, S. Mühlbrandt, M. Korbman, J. Reichert, M. Schultze, S. Holzner, J. V. Barth, R. Kienberger, R. Ernstorfer, V. S. Yakovlev, M. I. Stockman, and F. Krausz, "Optical-field-induced currents in dielectrics," Nature **493**, 70–74 (2013).
10. T. Higuchi, C. Heide, K. Ullmann, H. B. Weber, and P. Hommelhoff, "Light-field-driven currents in graphene," Nature **550**, 224–228 (2017).
11. S. Sederberg, D. Zimin, S. Keiber, F. Siegrist, M. S. Wismer, V. S. Yakovlev, I. Floss, C. Lemell, J. Burgdörfer, M. Schultze, F. Krausz, and N. Karpowicz, "Attosecond optoelectronic field measurement in solids," Nat. Commun. **11**, 430 (2020).
12. D. J. Cook and R. M. Hochstrasser, "Intense terahertz pulses by four-wave rectification in air," Opt. Lett. **25**, 1210–1212 (2000).
13. T. Löffler, F. Jacob, and H. G. Roskos, "Generation of terahertz pulses by photoionization of electrically biased air," Appl. Phys. Lett. **77**, 453–455 (2000).
14. M. Kress, T. Löffler, S. Eden, M. Thomson, and H. G. Roskos, "Terahertz-pulse generation by photoionization of air with laser pulses composed of both fundamental and second-harmonic waves," Opt. Lett. **29**, 1120–1122 (2004).
15. T. Löffler, M. Kress, M. Thomson, and H. G. Roskos, "Efficient terahertz pulse generation in laser-induced gas plasmas," Acta Phys. Pol. A **107**, 99–108 (2005).
16. X. Xie, J. Dai, and X.-C. Zhang, "Coherent control of THz wave generation in ambient air," Phys. Rev. Lett. **96**, 075005 (2006).
17. H. Zhong, N. Karpowicz, and X.-C. Zhang, "Terahertz emission profile from laser-induced air plasma," Appl. Phys. Lett. **88**, 261103 (2006).
18. K. Y. Kim, J. H. Glownia, A. J. Taylor, and G. Rodriguez, "Terahertz emission from ultrafast ionizing air in symmetry-broken laser fields," Opt. Express **15**, 4577–4584 (2007).

19. J. Hebling, K.-L. Yeh, M. C. Hoffmann, B. Bartal, and K. A. Nelson, "Generation of high-power terahertz pulses by tilted-pulse-front excitation and their applications possibilities," J. Opt. Soc. Am. B **25**, B6–B19 (2008).
20. H. Hirori, A. Doi, F. Blanchard, and K. Tanaka, "Single-cycle terahertz pulses with amplitude exceeding 1 MV/cm generated by optical rectification in $LiNbO_3$," Appl. Phys. Lett. **98**, 091106 (2011).
21. L. Guiramand, J. E. Nkeck, X. Ropagnol, T. Ozaki, and F. Blanchard, "Near-optimal intense and powerful terahertz source by optical rectification in lithium niobate crystal," arXiv:2104.10804 (2021).
22. F. Blanchard, L. Razzari, H.-C. Bandulet, G. Sharma, R. Morandotti, J.-C. Kieffer, T. Ozaki, M. Reid, H. F. Tiedje, H. K. Haugen, and F. A. Hegmann, "Generation of 1.5 mJ single-cycle terahertz pulses by optical rectification from a large-aperture ZnTe crystal," Opt. Express **15**, 13212–13220 (2007).
23. M. Shalaby, C. Vicario, K. Thirupugalmani, S. Brahadeeswaran, and C. P. Hauri, "Intense THz source based on BNA organic crystal pumped at Ti:sapphire wavelength," Opt. Express **41**, 1777–1780 (2016).
24. E. Isgandarov, X. Ropagnol, M. Singh, and T. Ozaki, "Intense terahertz generation from photoconductive antennas," Front. Optoelectron. **14**, 64–93 (2021).
25. I. Dey, K. Jana, V. Y. Fedorov, A. D. Koulouklidis, A. Mondal, M. Shaikh, D. Sarkar, A. D. Lad, S. Tzortzakis, A. Couairon, and G. R. Kumar, "Highly efficient broadband terahertz generation from ultrashort laser filamentation in liquids," Nat. Commun. **8**, 1184 (2017).
26. A. D. Koulouklidis, C. Gollner, V. Shumakova, V. Y. Fedorov, A. Pugzlys, A. Baltuska, and S. Tzortzakis, "Observation of extremely efficient terahertz generation from mid-infrared two-color laser filaments," Nat. Commun. **11**, 292 (2020).
27. N. Karpowicz and X.-C. Zhang, "Coherent terahertz echo of tunnel ionization in gases," Phys. Rev. Lett. **102**, 093001 (2009).
28. D. Zhang, Z. Lü, C. Meng, X. Du, Z. Zhou, Z. Zhao, and J. Yuan, "Synchronizing terahertz wave generation with attosecond bursts," Phys. Rev. Lett. **109**, 243002 (2012).
29. C. Meng, W. Chen, X. Wang, Z. Lü, Y. Huang, J. Liu, D. Zhang, Z. Zhao, and J. Yuan, "Enhancement of terahertz radiation by using circularly polarized two-color laser fields," Appl. Phys. Lett. **109**, 131105 (2016).
30. M. Kubullek, Z. Wang, K. von der Brelje, D. Zimin, P. Rosenberger, J. Schötz, M. Neuhaus, S. Sederberg, A. Staudte, N. Karpowicz, M. F. Kling, and B. Bergues, "Single-shot carrier-envelope-phase measurement in ambient air," Optica **7**, 35–39 (2020).
31. A. Korobenko, K. Johnston, M. Kubullek, L. Arissian, Z. Dube, T. Wang, M. Kübel, A. Y. Naumov, D. M. Villeneuve, M. F. Kling, P. B. Corkum, A. Staudte, and B. Bergues, "Femtosecond streaking in ambient air," Optica **7**, 1372–1376 (2020).
32. D. Zimin, M. Weidman, J. Schötz, M. F. Kling, V. S. Yakovlev, F. Krausz, and N. Karpowicz, "Petahertz-scale nonlinear photoconductive sampling in air," Optica **8**, 586–590 (2021).
33. A. Couairon and A. Mysyrowicz, "Femtosecond filamentation in transparent media," Phys. Rep. **441**, 47–189 (2007).
34. M. Porer, J.-M. Ménard, and R. Huber, "Shot noise reduced terahertz detection via spectrally postfiltered electro-optic sampling," Opt. Lett. **39**, 2435–2438 (2014).
35. S. Keiber, S. Sederberg, A. Schwarz, M. Trubetskov, V. Pervak, F. Krausz, and N. Karpowicz, "Electro-optic sampling of near-infrared waveforms," Nat. Photonics **10**, 159–162 (2016).
36. S. Sederberg, F. Kong, F. Hufnagel, C. Zhang, E. Karimi, and P. B. Corkum, "Vectorized optoelectronic control and metrology in a semiconductor," Nat. Photonics **14**, 680–685 (2020).
37. K. Jana, K. R. Herperger, F. Kong, Y. Mi, C. Zhang, P. B. Corkum, and S. Sederberg, "Reconfigurable electronic circuits for magnetic fields controlled by structured light," Nat. Photonics **15**, 622–626 (2021).
38. K. Jana, E. Okocha, S. H. Møller, Y. Mi, S. Sederberg, and P. B. Corkum, "Reconfigurable terahertz metasurfaces coherently controlled by wavelength-scale-structured light," Nanophotonics (2021).
39. R. W. Hellwarth and P. Nouchi, "Focused one-cycle electromagnetic pulses," Phys. Rev. A **54**, 889–895 (1996).
40. M. Borghesi, A. J. Mackinnon, A. R. Bell, R. Gaillard, and O. Willi, "Megagauss magnetic field generation and plasma jet formation on solid targets irradiated by an ultraintense picosecond laser pulse," Phys. Rev. Lett. **81**, 112–115 (1998).
41. M. Shaikh, A. D. Lad, K. Jana, D. Sarkar, I. Dey, and G. R. Kumar, "Megagauss magnetic fields in ultra-intense laser generated dense plasmas," Plasma Phys. Controlled Fusion **59**, 014007 (2017).